*Desalination and Water Treatment*
www.deswater.com

doi: 10.1080/19443994.2015.1028456

57 (2016) 9474–9487
April

Taylor & Francis
Taylor & Francis Group

# Characterization and adsorption kinetic study of surfactant treated oil palm (*Elaeis guineensis*) empty fruit bunches

Mohammed Danish[a,*], Tanweer Ahmad[b], Rokiah Hashim[a], Mohd Ridzuan Hafiz[a], Arniza Ghazali[a], Othman Sulaiman[a], Salim Hiziroglu[c]

[a]*Bioresource Research Lab., Bioresource, Paper & Coatings Division, School of Industrial Technology, Universiti Sains Malaysia, Penang 11800, Malaysia, Tel. +60 46534302; Fax: +60 4657 3678; email: mdanishchem@gmail.com (M. Danish), Tel. +60 46535707; email: hrokiah@usm.my (R. Hashim), Tel. +60 46535219; emails: m.ridzuanhafiz@yahoo.com (M.R. Hafiz), arniza@usm.my (A. Ghazali), Tel. +60 46534302; email: othman@usm.my (O. Sulaiman)*
[b]*Department of Chemistry, School of Natural Science, Madawalabu University, Bale-Robe, Ethiopia, Tel. +251 936649947; email: tanweerakhan@gmail.com*
[c]*Natural Resource Ecology and Management, Oklahoma State University, Stillwater 74078 6013 OK, USA, Tel. +405 744 5445; email: salim.hiziroglu@okstate.edu*

Received 15 July 2014; Accepted 7 March 2015

ABSTRACT

Oil palm (*Elaeis guineensis*) empty fruit bunches (OPEFB) was treated with cetyltrimethylammonium bromide (CTAB) to make its surface suitable for methyl orange (MO) dye adsorption. CTAB-treated OPEFB samples were characterized for their surface functional groups using FTIR, pHzpc, proton-binding capacity, and Boehm titration techniques. The surface morphology and elemental composition of the sample were also studied, employing field emission scanning electron microscopy and energy dispersive X-ray spectroscopy (EDS). It was found that in totality, acidic surface functional group increased after CTAB treatment. The adsorption process was well explained with pseudo-second-order kinetic model. The obtained equilibrium sorption data were then analyzed using the Langmuir, Freundlich, Dubinin–Radushkevich, and Tempkin isotherms. The results showed that sorption was surfactant dose dependent and adsorption increased with an increase in the percentage of surfactant applied on the OPEFB. The maximum adsorption of MO was found at 1% surfactant treatment dose. It was also determined that MO adsorption onto the OPEFB treated with 1% CTAB solution (1% CTAB-OPEFB) followed the monolayer (Langmuir) adsorption. The maximum adsorption capacity of 1% CTAB-OPEFB for the removal of MO was found to be 18.08 mg/g at 298 K (at pH 6.3). Thermodynamic study revealed that the adsorption process was spontaneous and exothermic in nature. There was no energy barrier to initiate the adsorption of MO dye on the CTAB-treated OPFB.

*Keywords:* Adsorption; Isotherm; Methyl orange; Oil palm empty bunches; Surfactant; Cetyltrimethylammonium bromide

*Corresponding author.

1944-3994/1944-3986 © 2015 Balaban Desalination Publications. All rights reserved.

## 1. Introduction

It is a known fact that the presence of dyes in a water system is hazardous to the environment and human beings. The discharge of dye effluents to the environment is becoming a major concern due to its toxicity. The sources of these dyes are different types of industries such as textiles, dye manufacturing, dyeing, and printing. These dyes can also consume the dissolved oxygen required by aquatic species. Many of them have direct toxicity to microbial populations and even can be toxic and carcinogenic to mammals. The complex aromatic structures of dyes make them more stable and more difficult to remove from the effluents. It is a general perception that water quality is greatly influenced by its color since dye is the first contaminant to be recognized in wastewater. The presence of even small amounts of dyes in water—less than 1 ppm for some dyes—is highly visible and undesirable [1]. Therefore, removal of dye has been a very important but challenging area of wastewater treatment. Several methods including biological and physicochemical technologies have been suggested to remove dyes from wastewater. These processes include coagulation, electro-coagulation, anaerobic treatment, flotation, filtration, ion exchange, membrane separation, adsorption, and advanced oxidation [2–4].

Currently, there is growing interest in using low-cost, commercially available materials for the adsorption of dyes. The utilization of agricultural wastes for the treatment of polluted water is also an attractive and promising option for the environment. A wide variety of agricultural waste materials are being used as low-cost alternatives to replace expensive adsorbents. Oil palm (*Elaeis guineensis*) agricultural wastes have gained wide attention as effective adsorbents due to its low cost and significant adsorption potential for the removal of various pollutants. Malaysia is one of the largest producers and exporters of palm oil in the world, accounting for 11% of the world's oils and fats production and 27% of export trade of oils and fats. With the growth of palm oil production in Malaysia, the amount of residues generated also show a corresponding increase. In Malaysia, oil palm industries are producing substantial quantities of non-oil palm biomass of about 90 million tons of lignocellulosic biomass each year. The empty fruit bunches represent about 9% of this total solid waste production [5,6]. Therefore, attention is given to utilize empty fruit bunches as an adsorbent to clean water.

Many physical and chemical treatments for surface modification of the adsorbent have been invented by the contemporary researchers to enhance the adsorption capacity for dyes removal. Adsorption capacity of agricultural waste is commonly high for cationic dyes, whereas anionic dyes have a relatively low adsorption capacity. This may be due to the fact that the waste's surface is usually negatively charged in natural water bodies, which does not benefit to adsorb anions [7]. Therefore, the surface of the agricultural wastes has to be modified to improve their adsorption capacities for anionic dyes. Therefore, the surfaces of these agricultural wastes are modified by cationic surfactant to improve the adsorption capacity. Recently, some agricultural wastes were modified by surfactant for the removal of anionic dyes, resulting in satisfying adsorption capacities [8–10]. Surface-active substance or surfactants are amphipathic substances with lyophobic and lyophilic groups making them capable of adsorbing at the interfaces between liquids, solids, and gasses. They form self-associated clusters, which normally lead to organized molecular assemblies, monolayers, micelles, vesicles, liposomes, and membranes. Depending upon the nature of hydrophilic group, they can be anionic, cationic, non-ionic, and zwitterionic. The critical micelle concentration (CMC) is the concentration of amphiphilic molecules in solution at which the formation of aggregates such as micelles, round rods, and lamellar structures, in the solution [11]. Due to these characteristics, surfactant-modified adsorbents are not only superior in terms of their removal efficiency than that of the conventional adsorbents, but also encourage selective adsorption [12].

The objective of this study was to improve the adsorption capacity of oil palm empty fruit bunches (OPEFB) to adsorb methyl orange (MO). The surface of the OPEFB was modified by impregnating it with the cationic surfactant cetyltrimethylammonium bromide (CTAB). Adsorption capacities of the OPEFB modified with CTAB were also examined under various conditions to evaluate adsorption capacity of MO. Adsorption behavior of the CTAB-modified OPEFB was examined in terms of adsorption isotherms.

## 2. Materials and methods

### 2.1. Adsorbent preparation

OPEFB (*E. guineensis*) was supplied by Sabutek Sdn. Bhd., Teluk Intan, Perak, Malaysia. The OPEFB was washed with distilled water to remove dust and soluble substances. The samples were soaked in 0.1 N HCl solution overnight followed by washing to remove all soluble acid impurities. Then, the washed OPEFB was again soaked in 0.1 M NaOH solution overnight followed by washing to remove all soluble base impurities. The samples were dried, ground, and

washed thoroughly with distilled water for several times and dried in an oven at a temperature of 60 ± 2°C for 48 h. Then, they were crushed and sieved to produce particles in the range of 150–200 μm size.

For modification of adsorbent, CTAB ($CH_3(CH_2)_{14}CH_2N^+(CH_3)_3Br^-$) (chemical structure shown in Scheme 1) analytical grade from Sigma–Aldrich was used. The OPEFB was modified by cationic surfactant CTAB. Ten grams of OPEFB and 100 mL of different percentage (0.5, 1.0 and 2.0%) CTAB solutions were added to a 500-mL conical flask. The mixture was agitated in a shaker machine for overnight at a speed of 120 rpm. In the next step, suspension was left undisturbed to separate the liquid and the OPEFB from each other. The liquid was discarded, and the modified OPEFB samples were washed with distilled water several times to remove superficially held surfactant and chloride ions. The modified samples were dried in a hot air oven at 343 K for 7 h. The samples of the adsorbents prepared with different percentage of surfactants were coded as 0.5% CTAB-OPEFB for 0.5% surfactant-treated sample, 1% CTAB-OPEFB for 1% surfactant-treated sample, and 2% CTAB-OPEFB for 2% surfactant-treated sample. The selection of modified OPEFB for further study was based on the adsorption performed on different percentage of surfactant.

### 2.2. Characterization of CTAB-modified OPEFB

Field emission scanning electron microscopy (FESEM) (Carl-Ziess SMT, Oberkochen, Germany) and energy dispersive X-ray spectroscopy (EDS) (Oxford INCA 400 Oxford Instruments Analytical, Bucks, UK) analysis were carried out on untreated OPEFB and CTAB-modified OPEFB samples to study their surface morphology before and after adsorption of MO.

Fourier-transformed infrared spectrophotometer (Nicolet AVATAR 380) was also employed to analyze the surface functional of the OPEFB and surfactant-modified (1% CTAB-OPEFB) adsorbent. The potassium bromide (KBr) was used in the ratio of 1:100 (sample to KBr weight ratio) with oven-dried sample to make pellets at a pressure of 10342.13 kPa for infrared analysis. The spectra were recorded by 64 scan with 4 $cm^{-1}$ resolution in the mid-infrared region.

The point of zero charge of OPEFB and 1% CTAB-OPEFB was determined using the method described in a study by Fiol and Villaescusa [13]. Suspensions of 6 g/L of the sample were put in contact with 0.03 M $KNO_3$ solutions adjusted at pH values of 2.04, 3.01, 4.06, 5.56, 7.6, 8.5, 9.3, and 10.4. The suspensions were agitated for 24 h in an orbital thermostat shaker (Protech, Model: 903) at 100 rpm. The change of pH (ΔpH) during equilibration was calculated. The pHzpc was the trough of the pH vs. |ΔpH| plot. The pHzpc of an adsorbent is an important characteristic that determines the pH at which the adsorbent surface has net electrical neutrality. At this value, the acidic or basic functional groups no longer contribute to the pH of the solution.

About 0.100 ± 0.0001 g of weighed amount of sample was taken into Erlenmeyer flask before 20 mL of 0.1 M NaCl solution was added as background electrolyte solution. Then, 1 mL of either 0.1 M HCl or 0.1 M NaOH solution was added to change the pH of the OPEFB sample and 0.1 M NaCl mixture. The flask was left for agitation at room temperature to attain the equilibrium level. The change in pH during attaining equilibrium was converted into proton-binding capacity ($Q$) (mmol/g) of the OPEFB sample using the following equation:

$$Q = \frac{(V_0 - V_t)}{m}([H]_i - [OH]_i - [H]_e + [OH]_e) \quad (1)$$

where $V_0$ and $V_t$ are the volumes (mL) of background electrolyte (0.1 M NaCl) and the titrant (0.1 M NaOH or 0.1 M HCl) added and $m$ is the mass of adsorbent (g). Substituents i and e refer to the initial and equilibrium concentration.

Boehm titration method was used to determine the number of oxygen surface functional group in the activated carbon. About 0.5 g of OPEFB sample was placed in conical flasks with 50 mL of following solutions: 0.1 M of sodium hydroxide, 0.1 M of hydrochloric acid, 0.1 M of sodium bicarbonate, and 0.05 M of sodium carbonate. The capped conical flasks were sealed with film and stirred for 24 h and filtered, after that 10 mL of each filtrate was titrated with HCl and NaOH depending upon the nature of titrant. The number of acidic sites of various types was calculated

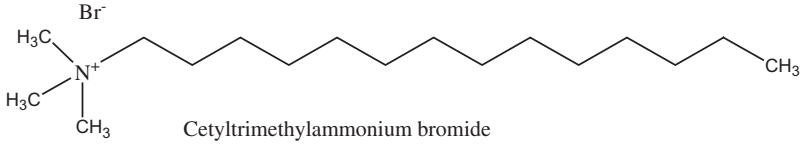

Cetyltrimethylammonium bromide

Scheme 1. Chemical structure of CTAB.

by presuming that sodium hydroxide neutralizes carboxylic, phenolic, and lactonic groups; sodium carbonate neutralizes carboxylic and lactonic groups; and sodium bicarbonate neutralizes only carboxylic groups. The number of basic sites was estimated by the amount of hydrochloric acid consumed by the carbon during stirring.

A modified method based on Boehm's technique was used to measure the cationexchange capacity (CEC) of the OPEFB samples. A weighed amount of sample (0.200 ± 0.0027 g) was placed into an Erlenmeyer flask. A volume of 50 mL of 0.1 M sodium hydroxide, 0.05 M sodium carbonate, and 0.1 M sodium hydrogen carbonate solutions was added. To attain equilibrium, the flasks were shaken for 24 h. After equilibration, the NaOH concentration was measured by titration with HCl. The quantity of NaOH consumed was converted to CEC and expressed in mmol/g using the following equation.

$$\mathrm{CEC} = \frac{(N_1 - N_2) \cdot V}{m} \tag{2}$$

where $N_1$ and $N_2$ are the normality of the NaOH solution before and after equilibrium, respectively; $V$ is the volume of NaOH taken in Erlenmeyer flask, and $m$ is mass of activated carbon used.

### 2.3. Adsorbate solutions

An anionic dye, MO ($C_{14}H_{14}N_3NaO_3S$) (chemical structure shown in Scheme 2), was purchased from Sigma-Aldrich and used without further purification. A stock solution of 1,000 mg/L was prepared by dissolving required amount of dye in double-distilled water which was later diluted to desired concentrations.

### 2.4. Batch adsorption studies

Previously prepared different percentages surfactant dose adsorbent (0.5% CTAB-OPEFB, 1% CTAB-OPEFB and 2% CTAB-OPEFB) masses of 0.1, 0.2, 0.3, 0.5, 0.7, 0.9, 1.0, and 1.5 g were taken separately for each percentage. The experiments were performed by adding the known weights of each adsorbent of 0.5% CTAB-OPEFB, 1% CTAB-OPEFB, and 2% CTAB-OPEFB into eight 250-mL capped conical flasks separately containing 50 mL of 100 ppm MO solution. For observing effect of temperature on adsorption, 0.7 g of 1% CTAB-OPEFB was kept in contact with 50 mL of 100 ppm MO dye solution at temperatures, ranging from 298 to 338 K in the temperature-controlled water bath. For observing the effect of initial concentration on adsorption, 0.7 g of 1% CTAB-OPEFB was kept in contact with 50 mL of MO dye solution with concentrations, ranging from 50 to 200 ppm at a fixed temperature of 298 K and pH of 6.3 inside a temperature control water bath. The conical flasks were shaken at 150 rpm for 24 h, and the equilibrium concentration of MO remaining in the solution phase was analyzed by UV–vis spectrophotometer (Shimadzu model UVmini 1240) at wavelength 464 Å.

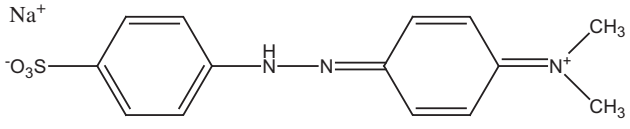


Methyl orange dye molecule in acidic solution

Scheme 2. Chemical structure of methyl orange dye in aqueous solution.

The percentage of MO adsorption and adsorption capacity at equilibrium, $q_e$, of the adsorbents was computed using below equations:

$$\%\ \text{adsorption} = \frac{(C_i - C_e) \times 100}{C_i} \tag{3}$$

$$q_t = \frac{(C_i - C_e) \times V}{W} \tag{4}$$

where $C_i$ and $C_e$ are the initial and equilibrium concentration of MO (mg/L) in the solution, $V$ is the volume of solution in mL, and $m$ is the mass of adsorbent taken in g units.

To quantify the applicability of proposed models, the correlation coefficients, $R^2$, were calculated from these plots. The linearity of these plots indicates the applicability of the models. Chi-square ($\chi^2$) test was also done to evaluate the best-fit adsorption model. The equation for evaluating the chi-square test to best fit the model is written as follows:

$$\chi^2 = \sum \frac{(q_t - q_{t(\mathrm{mod})})}{q_{t(\mathrm{mod})}} \tag{5}$$

## 3. Results and discussion

### 3.1. Characterization results of CTAB-modified OPEFB

The effect of percentage of surfactant that used to modify the OPEFB surface was studied in this work.

The surfactant percentage was taken 0.5, 1.0, and 2.0% onto dry weight of OPEFB. The obtained 0.5% CTAB-OPEFB, 1% CTAB-OPEFB, and 2% CTAB-OPEFB were evaluated for the effect of percentage surfactant on efficiency of adsorption. Fig. 1 shows the removal of MO by 0.5% CTAB-OPEFB, 1% CTAB-OPEFB, and 2% CTAB-OPEFB as well as OPEFB. The dosages of adsorbents were taken in the range of 0.1–0.7 g with initial concentration of 100 mg/L of MO dye solution. The adsorption experiments were conducted at temperature 298 K. No significant amount of dye was removed by pristine OPEFB as can be seen in Fig. 1. The adsorbents (OPEFB) modified with different percentage of surfactant (CTAB) as mentioned previously were also investigated for adsorption of MO. It was observed that with the rise of percentage of surfactant onto the OPEFB, the adsorption capacity increases, from 0.5 to 1% much rise was observed, but from 1 to 2% only small rise in adsorption capacity was observed. Based on the experiments, it could be concluded that at 1% surfactant (CTAB), dose was sufficient for the saturation of surfactant on the surface of OPEFB. In view of these findings, 1% CTAB-OPEFB was selected as optimized adsorbent for further study.

Fig. 2 illustrates the FESEM micrographs of OPEFB adsorbents before and after CTAB treatment. After 1% CTAB treatment, the ditches on the surface of OPEFB remains and there was not much morphological change in the surface image as can be seen in figure (Fig. 2). The EDS studies of OPEFB and 1% CTAB-modified OPEFB are shown in Fig. 3. After CTAB treatment, the percentage carbon on the surface of adsorbent increased from 49.7 to 52.3%.

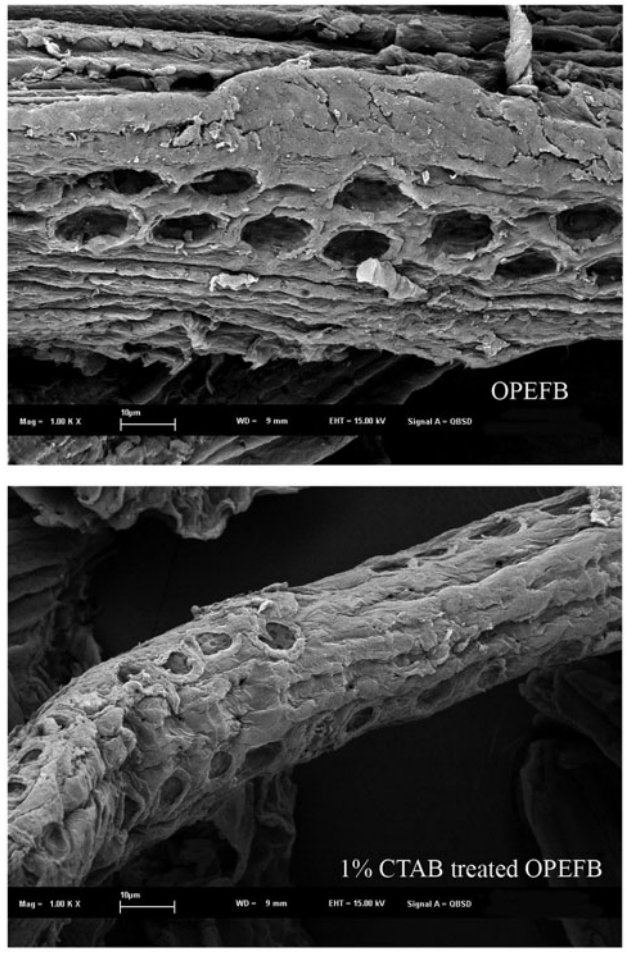


Fig. 2. FESEM micrographs of OPEFB and 1% CTAB-OPEFB.

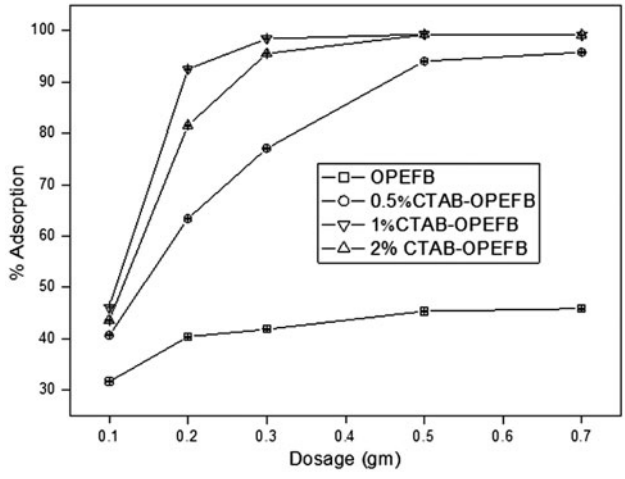


Fig. 1. Effect of adsorbent dosage for the adsorption of MO on different % CTAB-modified OPEFB.

The FTIR spectra of the samples as well as starting materials are shown in Fig. 4, and the spectra compare the presence of functional groups in parent materials, OPEFB and CTAB, and after combination of these two kinds of materials, the resultant change in functional groups occurs at the surface of adsorbent (1% CTAB-OPEFB). It can be seen from the spectra that multiple peaks are exhibited by the samples that indicate the presence of long molecular chains in the samples. For OPEFB and 1% CTAB-OPEFB, there is no major change in the number of peaks, because the major part of adsorbent (1% CTAB-OPEFB) contains OPEFB, and only 1% CTAB is present in it. Therefore, only minor broadening of the peak was observed. But this minor change in the surface functional groups plays a major role in MO adsorption. The Fourier-transformed infrared measurement for the 1% CTAB-OPEFB showed the presence of following functional groups: –OH (broad peak at 3,419, 3,570–3,200 $cm^{-1}$), methylene

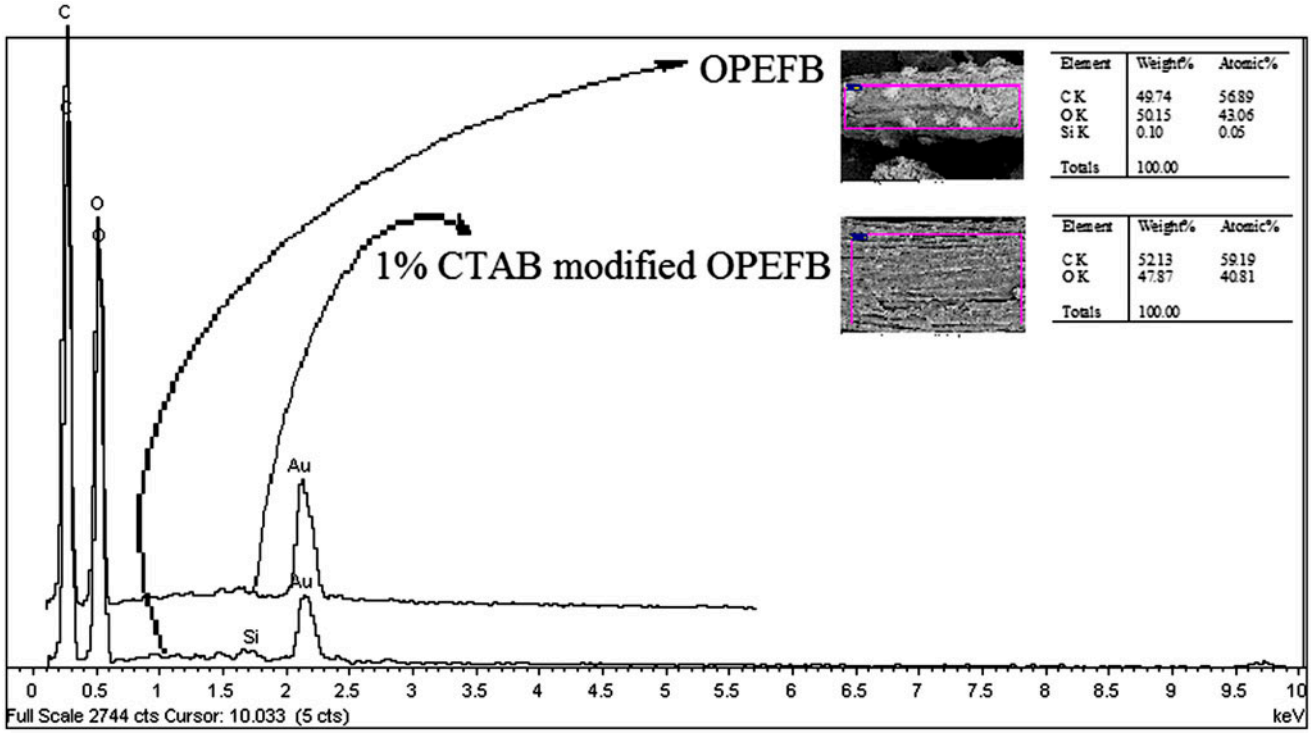


Fig. 3. EDS spectrum for OPEFB and 1% CTAB-OPEFB.

C–H asym./sym. stretching (2,935–2,915, 2,918 $cm^{-1}$), $–COONH_2$ (1,680–130, 1,643 $cm^{-1}$), carboxylate (1,420–1,300 $cm^{-1}$), tertiary CN– stretch (1,165 $cm^{-1}$), –C–C– skeletal vibrations (1,350–1,000 $cm^{-1}$), and C–H out of plane bend (897 $cm^{-1}$) [14].

The pH of the solution affected the surface charge of the adsorbents as well as the degree of ionization of dyes. The hydrogen ion and hydroxyl ions were absorbed quite strongly, and therefore, the adsorption of other ions was affected by the pH of the solution. The pHzpc values of OPEFB and 1% CTAB-OPEFB were found to be 3.5 and 3.3, respectively. It can be deduced from the result that pHzpc was reduced after CTAB modification of OPEFB. The small difference in pHzpc could be due to using very low percentage of surfactant (1% of CTAB) to modify OPEFB. The proton-binding capacity and cation exchange capacity increased after CTAB modification (values are shown in Table 1). These small changes in characteristics were found much effective for MO adsorption onto 1% CTAB-OPEFB surface.

The changes occur after CTAB treatment on OPEFB as described above were further investigated by the Boehm titration method. The results of Boehm titration are presented in Table 1. It was found that carboxylic and lactonic groups decreased, whereas phenolic and acidic groups (other than carboxylic and lactonic) increased after CTAB treatment. When the results are compared, the pristine OPEFB and CTAB treated OPEFB (1% CTAB-OPEFB). After CTAB treatment, no changes were observed on basic functional groups of OPEFB. These results show that the CTAB probably interact with the acidic functional groups (carboxylic and lactonic) of OPEFB and create some suitable functional groups that enhance the adsorption of MO.

### 3.2. Adsorption studies of the MO dye

Effect of adsorbent dosage on the percent adsorption was conducted to evaluate the efficiency of adsorption at a different amount of adsorbent. Fig. 5 shows the removal of MO by 1% CTAB-OPEFB, using different dosage of adsorbent (0.1–1.5 g) at initial concentration of 100 mg/L of MO solution and 25°C. From the figure, it was observed that the percentage of MO removal increased from 48.24 to 99.34% with an increase in adsorbent dosage from 0.1 to 0.7 g and further increase in adsorbent dose was not much effective in percentage MO removal. Hence, 0.7 g of 1% CTAB-OPEFB was selected as optimum weight for isotherm study. The initial increase in adsorption of

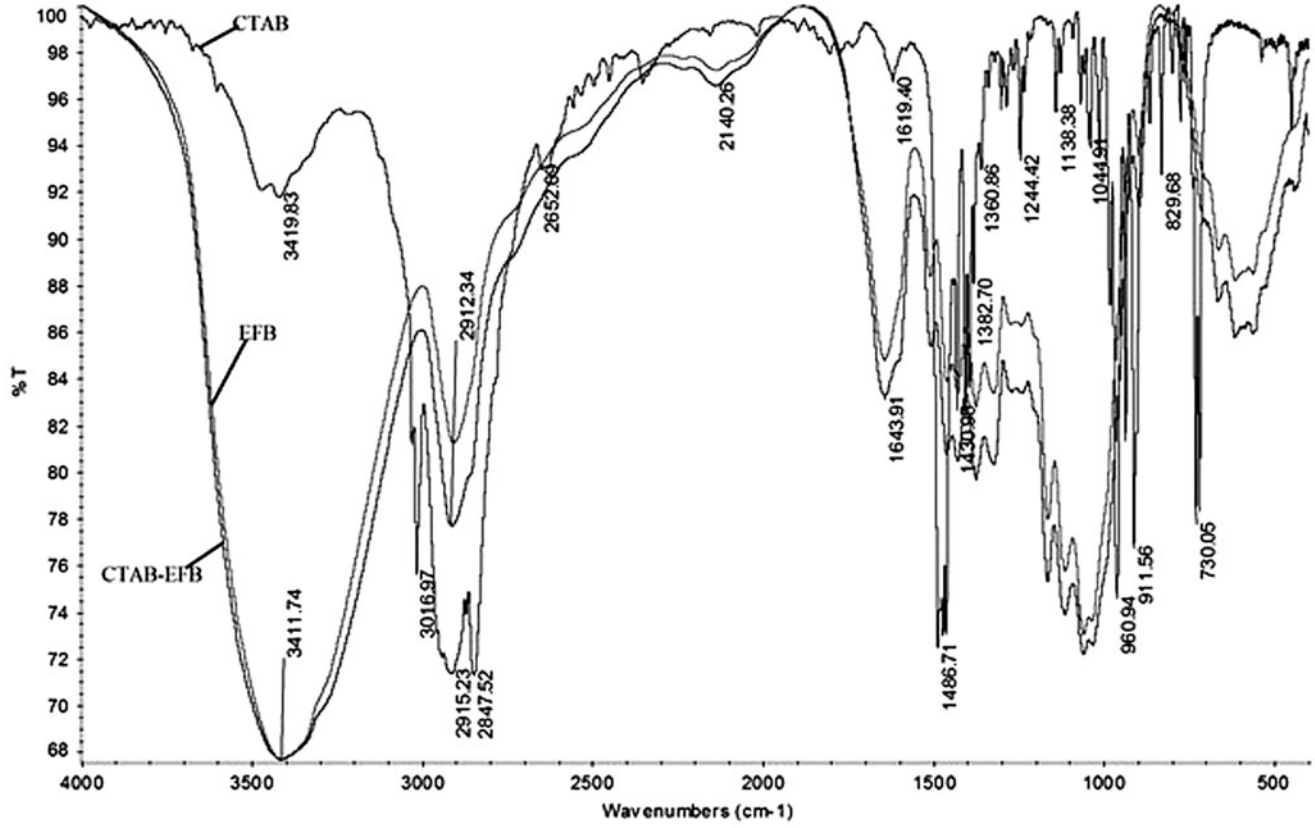


Fig. 4. FTIR spectra of CTAB, OPEFB, and 1% CTAB-OPEFB.

Table 1
Characterization of OPEFB and 1% CTAB-treated OPEFB

| | OPEFB | 1% CTAB-OPEFB |
|---|---|---|
| *Parameters* | | |
| pHzpc | 3.5 | 3.3 |
| Proton-binding capacity (mmol/g) | 0.0053 ± 0.0018 | 0.0134 ± 0.0020 |
| Cation exchange capacity (mmol/g) | 1.89 ± 0.38 | 2.13 ± 0.14 |
| *Boehm titration results* | | |
| Carboxylic (mmol/g) | 0.181 | 0.084 |
| Lactonic (mmol/g) | 0.868 | 0.448 |
| Phenolic (mmol/g) | 0.055 | 0.430 |
| Basic groups (mmol/g) | 0.022 | 0.022 |
| Acidic groups (mmol/g) | 1.680 | 1.931 |
| Total (mmol/g) | 1.702 | 1.953 |

MO with adsorbent dosage can be attributed to the availability of more adsorption sites due to CTAB association with OPEFB surface.

Adsorption of cationic surfactant from solution onto solid surfaces has undergone extensive study in recent years. Several mechanisms were proposed to the adsorption of cationic surfactants onto solid surfaces [15,16]. The nonpolar portion of CTAB most likely interacts with OPEFB surface through hydrophobic bonding, and the polar-charged head groups pointed toward the bulk of the solution, making the surface potential positive. In solution, certain groups in the OPEFB, such as lignin and cellulose, loose hydrogen ions and form a particle surface with a negative potential [17]. Therefore, another possible mechanism was the electrostatic attraction of surfactant cations onto the OPEFB surface, which offered a negative charge. As the concentration of surfactant will reach above the CMC [18], adsorption increases through hydrophobic interaction between hydrocarbon chains of the surfactant in the solution and the surfactant molecules already adsorbed on the surface. In both mechanisms, the surface got a positive potential, which was conducive to the removal of anionic dyes.

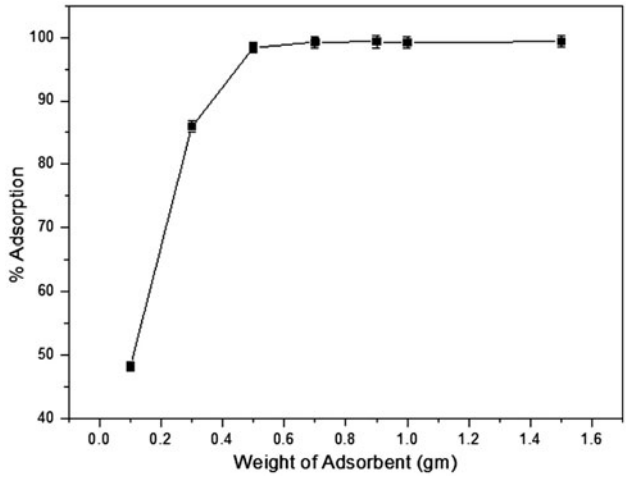


Fig. 5. Effect of adsorbent (1% CTAB-OPEFB) dosage for the adsorption of MO.

### 3.3. Kinetics of MO dye adsorption

In this study, the rate of removal of MO dye from aqueous solution by 1% CTAB-OPEFB was evaluated. It was evident that the solute uptake rate controls the residence time of adsorbate uptake at the solid–liquid interface including the diffusion process. The mechanism of adsorption depends on the physical and chemical characteristics of the adsorbents and on the mass transfer process. The removal of MO dye against time obtained from adsorption experiments was used to study the kinetics of MO adsorption. The rate of the adsorption of MO onto 1% CTAB-OPEFB was applied to the Lagergren pseudo-first-order model [19], pseudo-second-order model [20], and Weber–Morris diffusion model [21]. The conformity between experimental data and the predicted values of the model was expressed by the correlation coefficient ($R^2$) and chi-square ($\chi^2$) test.

#### 3.3.1. Pseudo-first-order kinetic model

The Lagergren pseudo-first-order rate model is based on the capacity of the adsorbent and is generally expressed as follows:

$$\frac{dq}{dt} = k_1(q_e - q_t) \tag{6}$$

where $q_e$ (mg/g) is the amount of solute adsorbed at equilibrium per unit weight of adsorbent, $q_t$ (mg/g) is the amount of solute adsorbed at a given time, and $k_1$ is the pseudo-first-order adsorption rate constant.

The Eq. (6) was integrated under the boundary conditions $t = 0$ to $t > 0$ ($q_t = 0$ to $q_t > 0$) and rearranged to obtain the following time-dependent function:

$$\log(q_e - q_t) = \log(q_e) - \left(\frac{k_1}{2.303}\right)t \tag{7}$$

The value of $k_1$ in the pseudo-first-order kinetic model and the corresponding correlation coefficients ($R^2$) and $\chi^2$ values were calculated and are summarized in Table 2.

The results showed that there is a large difference between the experimental adsorption capacity ($q_e$ = 7.119 mg/g) and adsorption capacity determined by the kinetic model ($q_e$ = 0.120 mg/g). Poor correlation coefficient value ($R^2$ = 0.4578) and very high $\chi^2$ value ($\chi^2$ = 422.4) indicate that this kinetics model cannot be predicted for adsorption of MO onto 1% CTAB-OPEFB.

#### 3.3.2. Pseudo-second-order kinetic model

The kinetic data were analyzed by applying the pseudo-second-order model to the experimental data. The pseudo-second-order kinetic model can be expressed as follows:

Table 2
Kinetic model for the adsorption of MO onto 1% CTAB-OPEFB

| | Values |
|---|---|
| *Kinetic models and its parameters* | |
| $q_{e,\ exp}$ (mg/g) | 7.119 |
| *Pseudo-first-order kinetic model* | |
| $q_{e,\ cal}$ (mg/g) | 0.12 |
| $k_1' \times 10^{-2}$ (1/min) | 0.392 |
| $\chi^2$ | 422.4 |
| $R^2$ | 0.4578 |
| *Pseudo-second-order kinetic model* | |
| $q_{e,\ cal}$ (mg/g) | 7.12 |
| $k_2 \times 10^{-2}$ (g/mg/min) | 60.74 |
| $h$ (mg/g/min) | 30.77 |
| $\chi^2$ | $5.6 \times 10^{-7}$ |
| $R^2$ | 1.000 |
| *Intra-particle diffusion* | |
| $k_{d1}$ (mg/g/min$^{1/2}$) | 1.9723 |
| $k_{d2}$ (mg/g/min$^{1/2}$) | 0.0011 |
| $C_1$ (mg/g) | 2.0397 |
| $C_2$ | 7.0814 |
| $R_1^2$ | 0.6227 |
| $R_2^2$ | 0.9186 |

$$\frac{dq}{dt} = k_1(q_e - q_t)^2 \quad (8)$$

After integrating Eq. (8) under the boundary conditions $t = 0$ to $t > 0$ and $q_t = 0$ to $q_t > 0$ and rearranging the equation, the following linearized form of the pseudo-second-order model was obtained.

$$\frac{t}{q_t} = \left(\frac{1}{k_2 q_e^2}\right) + \left(\frac{1}{q_e}\right)t \quad (9)$$

$$h = k_2 q_e^2 \quad (10)$$

where $h$ (mg/g/min) is the initial sorption rate. A plot of $t/q_t$ vs. t should produce a straight line, and the values of $q_e$ (mg/g) and $k_2$ (g/mg/min) can be determined from the slope and intercept of the plot.

The values of $k_2$, $q_e$, and $h$ are presented in Table 2, along with the corresponding correlation coefficients ($R^2$) and $\chi^2$ test values. The correlation coefficient ($R^2$) for this model was absolute ($R^2 = 1.00$), and $\chi^2$ test values ($\chi^2 = 5.6 \times 10^{-7}$) were very low which indicate that the model provided a perfect fit of the experimental data. The experimental adsorption capacity and pseudo-second-order model-based adsorption capacity was 7.119 and 7.120 mg/g, respectively. Thus, it can be concluded that the adsorption of MO onto 1% CTAB-OPEFB perfectly follows the pseudo-second-order kinetic model.

#### 3.3.3. Weber–Morris diffusion model

The possibility of intra-particle diffusion was examined by applying the Weber–Morris diffusion model to the experimental data. According to the Weber–Morris diffusion model, the amount of adsorbed material is proportional to the square root of the contact time,

$$q_t = k_d t^{1/2} + C \quad (11)$$

where $k_{d1}$ and $k_{d2}$ (mg/g/ $\text{min}^{1/2}$) are the intra-particle diffusion constant and $C_1$ and $C_2$ are the thickness of the boundary layer which was calculated from intercept of the plot of Eq. (11) in units of mg/g.

The Eq. (9) was applied to the adsorption data obtained at various contact times. The shape of plot indicated that the diffusion takes place in two steps. The rate of diffusion and the boundary thickness was calculated in each step. It was found that initially, the diffusion rate ($k_{d1} = 1.9723$ mg/g/$\text{min}^{1/2}$) was high with small boundary thickness ($C_1 = 2.0397$ mg/g), and second phase of adsorption has low diffusion rate ($k_{d1} = 0.0011$ mg/g/$\text{min}^{1/2}$) and large boundary thickness ($C_2 = 7.0814$ mg/g). The rate constant for intra-particle diffusion and the correlation coefficient was calculated from the respective plots and are displayed in Table 2.

### 3.4. Isotherm studies

The adsorption behavior of 1% CTAB-OPEFB for the removal of MO from aqueous solution was quantified with the Freundlich, Langmuir, Dubinin–Raduskevich (D–R), and Tempkin isotherm models.

#### 3.4.1. Freundlich adsorption isotherm model

The Freundlich model can be applied for non-ideal adsorption on heterogeneous surfaces and multilayer adsorption [22]. According to this model:

$$q_e = K_F[C_e]^{1/n} \quad (12)$$

$$\ln q_e = \ln K_F + \frac{1}{n}\ln[C_e] \quad (13)$$

where $C_e$ (mg/L) is the equilibrium concentration and $q_e$ (mg/g) is the amount adsorbed per specified amount of adsorbent, $K_F$ is Freundlich equilibrium constant, and $n$ is an empirical constant.

For the Freundlich isotherm, the plot of ln $q_e$ vs. ln $C_e$ gives a straight line with a slope $1/n$ and an intercept of ln $k_F$. This model deals with the multilayer adsorption of the adsorbate onto the adsorbent. The related parameters were calculated and presented in Table 3. The Freundlich type adsorption isotherm is an indication of surface heterogeneity of the adsorbent and thus is responsible for multilayer adsorption due to the presence of energetically heterogeneous adsorption sites. For the present study, it can be seen from Fig. 6 that experimental data points were not following the model trend line. Hence, it can be concluded that MO adsorption onto 1% CTAB-OPEFB was not following the Freundlich isotherm model.

#### 3.4.2. Langmuir adsorption isotherm model

This model assumes that the adsorptions occur at specific homogeneous sites on the adsorbent and are used successfully in many monolayer adsorption processes [23]. The data of the equilibrium studies for adsorption of MO onto 1% CTAB-OPEFB may follow the following form of Langmuir model:

Table 3
Adsorption isotherm constants and correlation coefficients for the adsorption of MO onto 1% CTAB-OPEFB at 25°C

| | Values |
|---|---|
| *Freundlich isotherm constants* | |
| $K_F$ (mg/g) | 9.481 |
| $n$ | 2.282 |
| $R^2$ | 0.789 |
| *Langmuir isotherm constants* | |
| $K_L$ (L/mg) | 1.333 |
| $q_m$ (mg/g) | 18.08 |
| $R_L$ | 0.003 |
| $R^2$ | 0.977 |
| *Dubinin–Radushkevich isotherm constants* | |
| $\beta \times 10^{-8}$ (mol$^2$/J$^2$) | 0.300 |
| $q_m$ (mg/g) | 16.15 |
| $E$ (kJ/mol) | 12.90 |
| $R^2$ | 0.802 |
| *Tempkin isotherm constants* | |
| $B_1$ (mg/g) | 3.972 |
| $K_T$ (mg/L) | 13.24 |
| $R^2$ | 0.909 |

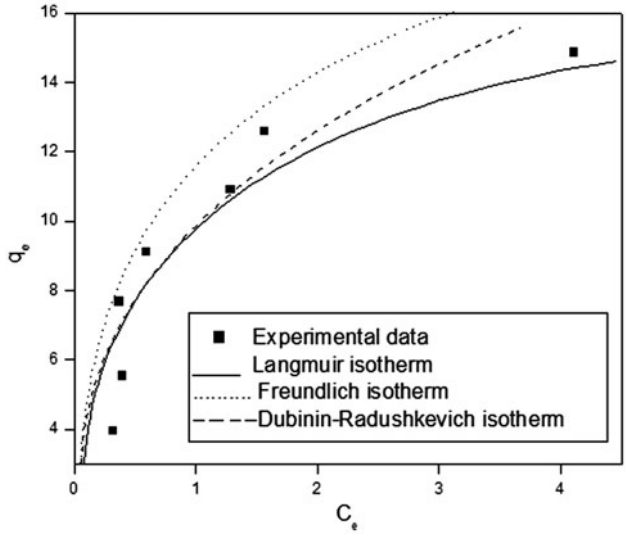


Fig. 6. Isotherm plot of $C_e$ vs. $q_e$ for the adsorption of MO onto 1% CTAB-OPEFB.

$$\frac{C_e}{q_e} = \left(\frac{1}{q_m K_L}\right) + \left(\frac{1}{q_m}\right) C_e \quad (14)$$

where $K_L$ (in units of L/mg) is the Langmuir equilibrium constant and $q_m$ (in units of mg/g) is the maximum amount of adsorbate required to form a monolayer. Hence, a plot of Ce/$q$e vs. Ce should be a straight line with a slope $(1/q_m)$ and an intercept as $(1/q_m K_L)$.

The adsorption isotherms revealed the specific relation between the concentration of the adsorbate and its adsorption degree onto adsorbent surface at a constant temperature. The applicability of the isotherm was judged by the correlation coefficient ($R^2$) values. The Langmuir type adsorption isotherm indicates surface homogeneity of the adsorbent and points toward the conclusion that the surface of adsorbent was made up of small adsorption patches which were energetically equivalent to each other in respect of adsorption phenomenon. When $C_e/q_e$ is plotted against $C_e$, a straight line with a slope $(1/K_L)$ and an intercept as $(1/q_m K_L)$ is obtained. The correlation coefficient ($R^2$) values of 0.977 indicated that the adsorption data of MO onto 1% CTAB-OPEFB were well fitted to the Langmuir isotherm. The values of constants $K_L$ and $q_m$ were calculated and reported in Table 3.

From Table 3, the Langmuir adsorption isotherm model yielded best fit as indicated by the highest $R^2$ values for all temperatures compared to the Freundlich adsorption isotherm model. Surfactant-modified 1% CTAB-OPEFB was found having a moderate adsorption capacity of 18.08 mg/g indicating that it could be considered as a promising material for the removal of MO from aqueous solutions.

For the investigation of favorable or unfavorable adsorption of MO onto 1% CTAB-OPEFB, the Langmuir model can be classified by a dimensionless constant, $R_L$. Mathematically, it can be defined by the following relation:

$$R_L = \frac{1}{(1 + K_L \cdot [C_0])} \quad (15)$$

where $K_L$ (L/g) is the Langmuir constant and $C_0$ (mg/L) is the highest initial MO concentration used for isotherm study. If the value of $R_L > 1$, the adsorption will be unfavorable; $R_L = 1$, the adsorption will be linear; $R_L < 1$, adsorption will be favorable; and $R_L = 0$, adsorption will be irreversible. The value of $R_L$ for MO adsorption onto 1% CTAB-OPEFB was 0.003 ($R_L < 1$), which indicates the favorable adsorption.

### 3.4.3. D–R isotherm models

The D–R model was applied to equilibrium data to determine the physical or chemical nature of the adsorption process [24]. The linearized form of the D–R model is given below:

$$\ln q_e = \ln q_m - \beta\varepsilon^2 \quad (16)$$

where $\beta$ ($mol^2/J^2$) is the activity coefficient related to mean adsorption energy and $\varepsilon$ ($kJ^2\ mol^2$) is the Polanyi potential.

The Polanyi potential [25] can be calculated using the following equation:

$$\varepsilon = RT\ \ln\left(1 + \frac{1}{C_e}\right) \quad (17)$$

The mean adsorption energy, $E$ (kJ/mol), is calculated with the help of the following equation:

$$E = \frac{1}{\sqrt{2\beta}} \quad (18)$$

The values are the mean free energy, $E$, the activity coefficient, $\beta$, and the correlation coefficient ($R^2$) and are reported in Table 3. The adsorption potential was independent of the temperature, but it depends upon the nature of the adsorbent and adsorbate. The mean free energy of the adsorption, $E$, provides information about the nature of adsorption whether it is a chemical ion exchange or physical adsorption. The values of $E$ that lie between 8 and 16 kJ/mol depict the adsorption process that follows the chemical ion exchange. The mean free energy for this adsorption was found to be 12.90 kJ/mol, which indicated that adsorption mechanism was followed by chemical ion exchange.

### 3.4.4. Tempkin isotherm models

The Tempkin isotherm is given as follows:

$$q_e = \frac{RT}{b}\ln\left(K_T C_e\right) \quad (19)$$

which can be linearized as follows:

$$q_e = B_1 \ln K_T + B_1 \ln C_e \quad (20)$$

where,

$$B_1 = \frac{RT}{b} \quad (21)$$

Table 4
Comparison of MO dye removal capacities through various adsorbents

| Adsorbent | $q_m$ (mg/g) MO | Adsorption condition Temp (K) | pH | Dose (g/L) | References |
|---|---|---|---|---|---|
| Physically activated *Acacia mangium* wood carbon in the presence of $CO_2$ gas | 7.5 | 298 | 6.30 | 1.6 | [27] |
| Chemically activated *Acacia mangium* wood carbon in the presence of $H_3PO_4$ | 196.3 | 328 | 6.27 | 0.5 | [28] |
| Raw bentonite | 34.3 | 295 | 4.00 | 1.25 | [29] |
| Banana peel | 17.2 | 303 | 6–7 | 1.00 | [30] |
| Orange peel | 15.8 | 303 | >7.0 | 1.00 | [30] |
| Ostrich bone CTABr | 722.8 | 298 | 6.5 | 1.00 | [31] |
| Ostrich bone SDBS | 54.1 | 298 | 6.5 | 1.00 | [31] |
| $BiFe_2O_3$/α-$Fe_2O_3$ composite | 5.8 | – | 5.2 | 10.0 | [32] |
| Chitosan-coated quartz sand (CCS) | 45.5 | 293 | 4.0 | 1.00 | [33] |
| Magnetic iron oxide nanoparticles (SPION) | 0.3 | – | 3.0 | – | [34] |
| SPION-MWCN | 10.5 | – | 3.0 | – | [34] |
| CTAB-modified wheat straw | 50.4 | 303 | 3.0 | 1.00 | [35] |
| Cork powder | 16.7 | 298 | 2.0 | 5.00 | [36] |
| Mesoporous carbon CMK-3 | 294.1 | 298 | 3–9 | 2.00 | [37] |
| *Moringa peregrine* tree shell ash | 14.0 | 293 | 2.0 | 13.0 | [38] |
| Activated clay | 15.9 | 293 | ≤7.0 | 5.0 | [39] |
| Natural skin almond (NSA) | 15.0 | 296 | 4.0 | 6.0 | [40] |
| $H_2SO_4$-treated skin almond (TSA) | 31.2 | 296 | 4.0 | 6.0 | [40] |
| Almond shell | 38.6 | 293 | 3.0 | 1.0 | [41] |
| HDTMAB-silkworm exuviae | 77.7 | 303 | 7.0 | 2.00 | [7] |
| CTAB-modified OPEFB | 18.1 | 298 | 6.3 | 14.0 | This study |

A plot of $q_e$ vs. ln $C_e$ enables the determination of the isotherm constants $B_1$ (mg/g) and $K_T$ (mg/L) from the slope and the intercept, respectively. $K_T$ is the equilibrium binding constant corresponding to the maximum binding energy. The $R$ and $T$ are the gas constant (8.314 J/mol/K) and the absolute temperature (K), respectively. The constant $b$ is related to the heat of adsorption.

The Tempkin isotherm contains a factor that explicitly takes into account the adsorbate and adsorbent interactions. This isotherm assumes that (i) the heat of adsorption of all the molecules in the layer decreases linearly with coverage because of adsorbent–adsorbate interactions and (ii) the adsorption is characterized by a uniform distribution of binding energies, up to some maximum binding energy [26]. For MO adsorption on to 1% CTAB-OPEFB, the maximum binding energy, $K_T$, and isotherm constant, $B_1$, were found 13.24 and 3.972 mg/g, respectively (Table 3).

We surveyed the literature to compare various adsorbents for their adsorption capacities of MO dye. Table 4 lists a comparison of maximum adsorption capacities of MO on various adsorbents at certain temperature and pH.

### 3.5. Thermodynamics of MO dye adsorption

The standard free energy change ($\Delta G^\circ$) is the fundamental criterion of spontaneity of a process and can be determined using thermodynamic equilibrium constant and temperature as shown below:

$$\Delta G^\circ = -RT \ln K_{eq} \quad (22)$$

where $R$ (8.314 J/mol/K) is the universal gas constant, $T$ (K) is the absolute temperature, and $K_{eq}$ is the thermodynamic equilibrium constant. Similarly, the standard enthalpy change ($\Delta H^\circ$) and standard entropy change ($\Delta S^\circ$) from 298.15 to 338.15 K was computed from the following equation.

$$\ln K_{eq} = \frac{\Delta S^\circ}{R} - \frac{\Delta H^\circ}{RT} \quad (23)$$

In order to evaluate the thermodynamic parameters for the adsorption of MO onto 1% CTAB-OPEFB, the adsorption studies were carried out at five different temperatures from 298.15 to 338.15 K. Thermodynamic equilibrium constant ($K_{eq}$) was calculated as the ratio of MO concentration adsorb onto 1% CTAB-OPEFB and concentration remain in solution. A plot of ln $K_{eq}$ vs. $1/T$ gave a straight line as shown in Fig. 7. The slope and intercept of the plot provides the values of

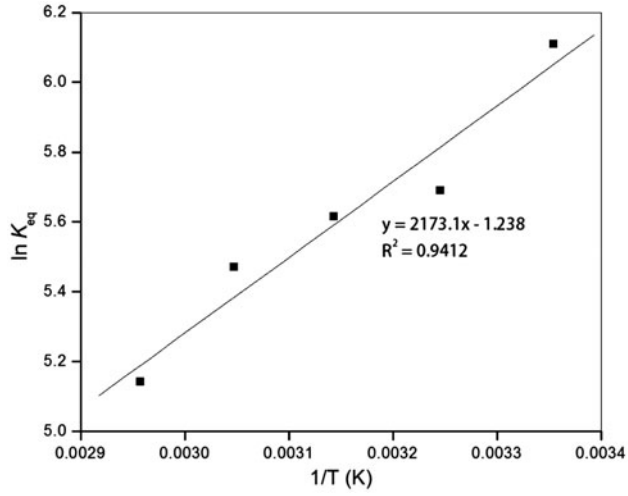


Fig. 7. van't Hoff plots for the adsorption of MO onto 1% CTAB-OPEFB.

Table 5
Values of thermodynamic parameters for the adsorption of MO onto 1% CTAB-OPEFB

| Temperature (K) | $\Delta G^\circ$ (kJ/mol) | $\Delta H^\circ$ (kJ/mol) | $\Delta S^\circ$ (kJ/mol/K) |
|---|---|---|---|
| 298.15 | −14.99 | | |
| 308.15 | −14.89 | | |
| 318.15 | −14.79 | −18.07 | −10.29 |
| 328.15 | −14.69 | | |
| 338.15 | −14.58 | | |

$\Delta H^\circ$ and $\Delta S^\circ$, respectively. The standard free energy change ($\Delta G^\circ$), standard enthalpy change ($\Delta H^\circ$), and standard entropy change ($\Delta S^\circ$) were obtained from the Eqs. ((22) and (23)), and its values associated with the adsorption of MO onto 1% CTAB-OPEFB are listed in Table 5. Negative values of $\Delta G^\circ$ indicated the feasibility of the process and spontaneous nature of the adsorption of MO onto 1% CTAB-OPEFB. Negative value of $\Delta H^\circ$ indicated the exothermic nature of the processes, while negative value of $\Delta S^\circ$ reflected the decrease in the randomness at the solid/liquid interface during the adsorption process.

## 4. Conclusions

The present study characterized the effect of CTAB treatment on the surface of OPEFB. The 1% CTAB-OPEFB was having proton-binding capacity and cation exchange capacity 0.0134 and 2.13 mmol/g, respectively. The carboxylic and lactonic groups in1% CTAB-OPEFB decreased to be 0.084 and

0.448 mmol/g, respectively, compare to pristine OPEFB (carboxylic group 0.181 mmol/g and Lectonic group 0.868 mmol/g). The adsorption kinetics studies of MO on 1% CTAB-OPEFB proved that pseudo-second order was a suitable kinetic model. Equilibrium data fitted very well in the Langmuir isotherm equation, confirming the monolayer adsorption capacity of MO onto 1% CTAB-OPEFB with adsorption capacity of 18.08 mg/g. Thermodynamic parameters, enthalpy change, entropy change, and Gibbs free energy change were also calculated for the removal of MO. These parameters showed that adsorption on the surface of 1% CTAB-OPEFB were feasible, spontaneous, and endothermic in nature. The mechanism of the adsorption was ion exchange in nature.

## Acknowledgments

The authors acknowledged Universiti Sains Malaysia for financial support through Research Grant Scheme (1001/PTEKIND/814048) to carry out this research and Post-Doctoral fellowship to Dr Mohammed Danish.

### Lists of symbols

$q_e$ — equilibrium adsorption capacity (mg/g)
$q_t$ — adsorption capacity at time-$t$ (mg/g)
$q_{t(\mathrm{mod})}$ — adsorption capacity at time-$t$ (mg/g) calculated through model
$q_m$ — maximum adsorption capacity (mg/g)
$N_1$ — normality of NaOH before adsorption
$N_2$ — normality of NaOH after adsorption
$[C_0]$ — highest initial methyl orange concentration (mg/L)
$C$ — boundary thickness
$C_1$ — first layer boundary thickness
$C_2$ — second layer boundary thickness
$C_e$ — equilibrium methyl orange concentration in solution (mg/L)
$C_i$ — initial methyl orange concentration (mg/L)
$C_t$ — adsorbate concentration at time-$t$ (mg/L)
$K_L$ — Langmuir sorption equilibrium constant (L/mg)
$R_L$ — separation factor (dimensionless quantity)
$k_F$ — Freundlich constant ($\mathrm{mg}^{1-n}/\mathrm{g/L}^n$)
$n$ — an empirical dimensionless constant measures nature and strength of the sorption process and the distribution of active sites
$\beta$ — activity coefficient related to mean adsorption energy ($\mathrm{mol}^2/\mathrm{J}^2$)
$\varepsilon$ — Polanyi potential ($\mathrm{kJ}^2\ \mathrm{mol}^2$)
$R$ — universal gas constant (8.314 J/K/mol)
$T$ — absolute temperature (K)
$E$ — mean free adsorption energy (kJ/mol)
$K_{eq}$ — chemical equilibrium constant
$B_1$ — Temkin isotherm constant
$K_T$ — maximum binding energy
$b$ — heat of adsorption
$\Delta G^\circ$ — standard Gibbs free energy (J/mol)
$\Delta S^\circ$ — standard change in entropy (J/K/mol)
$\Delta H^\circ$ — standard change in enthalpy (J/mol)
$t$ — time in minute
$k_1$ — pseudo-first-order kinetics rate constant (1/min.)
$k_2$ — pseudo-second-order kinetics rate constant (g/mg/min)
$h$ — initial sorption rate (mg/g/min)
$k_d$ — intra-particle diffusion rate constant ($\mathrm{mg/g/min}^{1/2}$)
$k_{d1}$ — first layer diffusion rate constant ($\mathrm{mg/g/min}^{1/2}$)
$k_{d2}$ — second layer diffusion rate constant ($\mathrm{mg/g/min}^{1/2}$)
$Q$ — proton-binding capacity (mmol/g)
$V_0$ — volume of background electrolyte (mL)
$V_t$ — volume of the titrant (0.1 M NaOH or 0.1 M HCl) (mL)
$m$ — mass of the adsorbent (g)
$[\mathrm{H}]_i$ — initial hydronium ion concentration (mol/L)
$[\mathrm{OH}]_i$ — initial hydroxyl ion concentration (mol/L)
$[\mathrm{H}]_e$ — hydronium ion concentration at equilibrium (mol/L)
$[\mathrm{OH}]_e$ — hydroxyl ion concentration at equilibrium (mol/L)
$V$ — volume of the adsorbate solution (mL)
$R^2$ — regression coefficient
$\chi^2$ — chi-square for statistical test

## References

[1] T. Robinson, G. McMullan, R. Marchant, P. Nigam, Remediation of dyes in textile effluent: A critical review on current treatment technologies with a proposed alternative, Bioresour. Technol. 77 (2001) 247–255.
[2] W. Delée, C. O'Neill, F.R. Hawkes, H.M. Pinheiro, Anaerobic treatment of textile effluents: A review, J. Chem. Technol. Biotechnol. 73 (1998) 323–335.
[3] H.S. Rai, M.S. Bhattacharyya, J. Singh, T.K. Bansal, P. Vats, U.C. Banerjee, Removal of dyes from the effluent of textile and dyestuff manufacturing industry: A review of emerging techniques with reference to biological treatment, Crit. Rev. Environ. Sci. Technol. 35 (2005) 219–238.
[4] S. Mondal, Methods of dye removal from dye house effluent—An overview, Environ. Eng. Sci. 25 (2008) 383–396.
[5] MPOB (Malaysian Palm Oil Board), Latest development and commercialization of oil palm biomass, Seminar on Business Opportunity in Oil Palm Biomass, 21 August, Selangor, 2003.
[6] T. Ahmad, M. Rafatullah, A. Ghazali, O. Sulaiman, R. Hashim, Oil palm biomass-based adsorbents for the removal of water pollutants—A review, J. Environ. Sci. Health. Part C 29 (2010) 177–222.

[7] H. Chen, J. Zhao, J. Wu, G. Dai, Isotherm, thermodynamic, kinetics and adsorption mechanism studies of methyl orange by surfactant modified silkworm exuviae, J. Hazard. Mater. 192 (2011) 246–254.
[8] C. Namasivayam, M.V. Sureshkumar, Anionic dye adsorption characteristics of surfactant-modified coir pith, a 'waste' lignocellulosic polymer, J. Appl. Polym. Sci. 100 (2006) 1538–1546.
[9] M.V. Sureshkumar, C. Namasivayam, Adsorption behavior of Direct Red 12B and Rhodamine B from water onto surfactant-modified coconut coir pith, Colloids Surf., A 317 (2008) 277–283.
[10] B.C. Oei, S. Ibrahim, S. Wang, H.M. Ang, Surfactant modified barley straw for removal of acid and reactive dyes from aqueous solution, Bioresour. Technol. 100 (2009) 4292–4295.
[11] M.J. Rosen, Surfactants and Interfacial Phenomenon, Wiley, New York, NY, 2004.
[12] M. Nadeem, A. Mahmood, S.A. Shahid, S.S. Shah, A.M. Khalid, G. McKay, Sorption of lead from aqueous solution by chemically modified carbon adsorbents, J. Hazard. Mater. 138 (2006) 604–613.
[13] N. Fiol, I. Villaescusa, Determination of sorbent point zero charge: Usefulness in sorption studies, Environ. Chem. Lett. 7 (2009) 79–84.
[14] J. Coates, Interpretation of infrared FTIR spectra, A practical approach, in: R.A. Meyers (Ed.) Encyclopedia of analytical Chemistry, Wiley, Chichester, 2000, pp. 1–23.
[15] Z. Li, R.S. Bowman, Counterion effects on the sorption of cationic surfactant and chromate on natural clinoptilolite, Environ. Sci. Technol. 31 (1997) 2407–2412.
[16] C. Namasivayam, M.V. Sureshkumar, Removal of chromium(VI) from water and wastewater using surfactant modified coconut coir pith as a biosorbent, Bioresour. Technol. 99 (2008) 2218–2225.
[17] B. Chen, C.W. Hui, G. McKay, Pore-surface diffusion modeling for dyes from effluent on pith, Langmuir 17 (2001) 740–748.
[18] Z. Li, C.A. Willms, K. Kniola, Removal of anionic contaminants using surfactant-modified palygorskite and sepiolite, Clay Miner. 51 (2003) 445–451.
[19] S. Lagergren, About the theory of so called adsorption of soluble substances, K. Sven. Vetensk. Akad. Handl. 24 (1898) 1–39.
[20] Y.S. Ho, G. McKay, A comparison of chemisorptions kinetic models applied to pollutant removal on various sorbents, Process Saf. Environ. Prot. 76B (1998) 332–340.
[21] W.J. Weber, J.C. Morris, Kinetics of adsorption on carbon from solution, J. Sanit. Eng. Div. Am. Soc. Civ. Eng. 89 (1963) 31–60.
[22] H. Freundlich, Ueber die adsorption in Loesungen, Z. Phys. Chem. 57 (1907) 385–470.
[23] I. Langmuir, The adsorption of gases on plane surfaces of glass, mica and platinum, J. Am. Chem. Soc. 40 (1918) 1361–1403.
[24] M.M. Dubinin, E.D. Zaverina, L.V. Radushkevich, Sorption and structure of activated carbons I. Adsorption of organic vapours, Zh. Fiz. Khim. 21 (1947) 1351–1362.
[25] M. Polanyi, Theories of the adsorption of gases. A general survey and some additional remarks, Trans. Faraday Soc. 28 (1932) 316–332.
[26] M.J. Tempkin, V. Pyzhev, Recent modification to Langmiur isotherms, Acta. Physiochim. USSR 12 (1940) 217–222.
[27] M. Danish, R. Hashim, M.N.M. Ibrahim, O. Sulaiman, Characterization of physically activated acacia mangium wood-based carbon for the removal of methyl orange dye, BioResources 8(3) (2013) 4323–4339.
[28] M. Danish, R. Hashim, M.N. Mohamad Ibrahim, O. Sulaiman, Response surface methodology approach for methyl orange dye removal using optimized *Acacia mangium* wood activated carbon, Wood Sci. Technol. 48(5) (2014) 1085–1105.
[29] E. Eren, Adsorption performance and mechanism in binding of azo dye by raw bentonite, CLEAN—Soil Air Water 38(8) (2010) 758–763.
[30] G. Annadurai, R.-S. Juang, D.-J. Lee, Use of cellulose-based wastes for adsorption of dyes from aqueous solutions, J. Hazard. Mater. 92 (2002) 263–274.
[31] M. Arshadi, A.R. Faraji, M.J. Amiri, M. Mehravar, A. Gil, Removal of methyl orange on modified ostrich bone waste—A novel organic–inorganic biocomposite, J. Colloid Interface Sci. 446 (2015) 11–23.
[32] W.J. Tseng, R.D. Lin, $BiFeO_3/\alpha$-$Fe_2O_3$ core/shell composite particles for fast and selective removal of methyl orange dye in water, J. Colloid Interface Sci. 428 (2014) 95–100.
[33] B.Zhao, X.Zhang, C.Dou, R.Han, Adsorption property of methyl orange by chitosan coated on quartz sand in batch mode, Desalin. Water Treat. (2014) 1–11, doi: 10.1080/19443994.2014.925834.
[34] Ş.S. Bayazit, Magnetic multi-wall carbon nanotubes for methyl orange removal from aqueous solutions: Equilibrium, kinetic and thermodynamic studies, Sep. Sci. Technol. 49(9) (2014) 1389–1400.
[35] Y. Su, Y. Jiao, C. Dou, R. Han, Biosorption of methyl orange from aqueous solutions using cationic surfactant-modified wheat straw in batch mode, Desalin. Water Treat. 52(31–33) (2013) 6145–6155.
[36] F. Krika, O.F. Benlahbib, Removal of methyl orange from aqueous solution via adsorption on cork as a natural and low-coast adsorbent: Equilibrium, kinetic and thermodynamic study of removal process, Desalin. Water Treat. (2014) 1–13.
[37] N. Mohammadi, H. Khani, V.K. Gupta, E. Amereh, S. Agarwal, Adsorption process of methyl orange dye onto mesoporous carbon material-kinetic and thermodynamic studies, J. Colloid Interface Sci. 362(2) (2011) 457–462.
[38] E. Bazrafshan, A.A. Zarei, H. Nadi, M.A. Zazouli, Adsorptive removal of methyl orange and reactive red 198 dyes by *Moringa peregrina* ash, Indian J. Chem. Technol. 21 (2014) 105–113.
[39] Q. Ma, F. Shen, X. Lu, W. Bao, H. Ma, Studies on the adsorption behavior of methyl orange from dye wastewater onto activated clay, Desalin. Water Treat. 51(19–21) (2013) 3700–3709.
[40] F. Atmani, A. Bensmaili, A. Amrane, Methyl orange removal from aqueous solutions by natural and treated skin almonds, Desalin. Water Treat. 22(1–3) (2010) 174–181.
[41] F. Deniz, Optimization of methyl orange bioremoval by *Prunus amygdalus* L. (almond) shell waste: Taguchi methodology approach and biosorption system design, Desalin. Water Treat. 51(37–39) (2013) 7067–7073.